

# Diffuse Gas in Galaxies Sheds New Light on the Origin of Type Ia Supernovae

Jonas Johansson<sup>1\*</sup>, Tyrone E. Woods<sup>1</sup>, Marat Gilfanov<sup>1,2</sup>, Marc Sarzi<sup>3</sup>, Yan-Mei Chen<sup>4,5</sup> and Kyuseok Oh<sup>6</sup>

<sup>1</sup>Max-Planck Institut für Astrophysik, Karl-Schwarzschild-Str. 1, D-85741 Garching, Germany

<sup>2</sup>Space Research Institute, Profsoyuznaya 84/32, 117997 Moscow, Russia

<sup>3</sup>Centre for Astrophysics Research, University of Hertfordshire, College Lane, Hatfield, Herts, AL10 9AB, UK

<sup>4</sup>Department of Astronomy, Nanjing University, Nanjing 210093, China

<sup>5</sup>Key Laboratory of Modern Astronomy and Astrophysics (Nanjing University), Ministry of Education, Nanjing 210093, China

<sup>6</sup>Department of Astronomy, Yonsei University, Seoul 120-749, Republic of Korea

19 June 2014

## ABSTRACT

We measure the strength of He II  $\lambda 4686$  nebular emission in passively evolving (“retired”) galaxies, aiming to constrain their populations of hot accreting white dwarfs (WDs) in the context of the single degenerate (SD) scenario of Type Ia supernovae (SNe Ia). In the SD scenario, as a WD burns hydrogen-rich material accreted from a companion star, it becomes a powerful source of ionizing UV emission. If significant populations of such sources exist in galaxies, strong emission in the recombination lines of He II should be expected from the interstellar medium. To explore this conjecture, we select from the Sloan Digital Sky Survey  $\sim 11\,500$  emission line galaxies with stellar ages  $> 1$  Gyr showing no signs of AGN activity and co-add their spectra in bins of stellar population age. For the first time, we detect He II  $\lambda 4686$  nebular emission in retired galaxies and find it to be significantly weaker than that expected in the SD scenario, especially in the youngest age bin ( $1 - 4$  Gyr) where the SN Ia rate is the highest. Instead, the strength of the observed He II  $\lambda 4686$  nebular emission is consistent with post-asymptotic giant branch stars being the sole ionizing source in all age bins. These results limit populations of accreting WDs with photospheric temperatures ( $T_{\text{eff}}$ ) in the range  $\sim (1.5 - 6) \cdot 10^5$  K to the level at which they can account for no more than  $\sim 5 - 10\%$  of the observed SN Ia rate. Conversely, should all WD progenitors of SN Ia go through the phase of steady nuclear burning with  $T_{\text{eff}} \sim (1.5 - 6) \cdot 10^5$  K, they do not increase their mass by more than  $\sim 0.03 M_{\odot}$  in this regime.

**Key words:** galaxies: ISM, elliptical and lenticular, cD – supernovae: general, white dwarfs

## 1 INTRODUCTION

The use of Type Ia supernovae (SNe Ia) as standard candles has been key to the discovery of the accelerating expansion of the Universe (Riess et al. 1998; Perlmutter et al. 1999). However, the nature of their progenitors remains uncertain, with increasing evidence suggesting they may arise through multiple evolutionary channels. This possible diversity, and the null detections of the progenitor of any individual SN Ia (e.g. Chomiuk 2013) have rendered population-based arguments a necessity.

The single-degenerate (SD) scenario (Whelan & Iben 1973) has long been one of the favoured progenitor channels for SNe Ia. In the classical picture, a carbon-oxygen white dwarf (WD) accretes mass from a co-orbiting binary companion, eventually exploding upon nearly reaching the critical Chandrasekhar mass ( $\sim 1.4 M_{\odot}$ ). Before this happens, steady nuclear burning of the accreted material occurs on the surface of the WD over an extended period of time ( $\sim 10^6$  yr) as soon as the mass transfer rate ( $\dot{M}$ ) exceeds a few times  $10^{-7} M_{\odot}/\text{yr}$  (Nomoto et al. 2007). For lower mass transfer rates, nuclear burning occurs only in unsteady flashes, expelling matter from the WD in nova outbursts (Prialnik & Kovetz 1995). This renders it difficult

\* E-mail: jjohansson@mpa-garching.mpg.de

for the WD to ever reach the Chandrasekhar mass, unless perhaps if accreting WDs undergo an extended evolutionary phase as recurrent novae binaries (Hachisu & Kato 2001). In the latter case, however, the SD scenario comes into conflict with statistics of classical/recurrent nova in the Andromeda galaxy (Soraisam & Gilfanov, in preparation).

Should all SNe Ia progenitors undergo a steady nuclear-burning phase during some fraction of the time prior to explosion, their total bolometric luminosity  $L_{tot}$  can easily be evaluated. It is proportional to the rate of exploding SN Ia ( $\dot{N}_{SNIA}$ ), and to the total amount of mass  $\Delta M_{SB}$  processed through steady burning, according to (Gilfanov & Bogdan 2010)

$$L_{tot} = \epsilon_H \chi \Delta M_{SB} \dot{N}_{SNIA}, \quad (1)$$

where  $\epsilon_H$  and  $\chi$  are the energy release per unit mass of hydrogen ( $\sim 6 \cdot 10^{18}$  erg/g) and the mass fraction of hydrogen ( $\sim 0.72$ ), respectively.

During steady nuclear-burning, the WD emits blackbody-like radiation with an effective temperature peaking around  $T_{eff} \sim (5 - 8) \cdot 10^5$  K, making it a prodigious source of soft X-ray emission ( $\sim 0.3 - 0.7$  keV, van den Heuvel et al. 1992). Given the observed rate of SNe Ia (Totani et al. 2008; Maoz, Mannucci & Brandt 2012; Graur et al. 2014), there should be a large number of accreting sources at any given time according to the SD scenario, sufficient to produce an integrated soft X-ray emission that would be detectable by modern X-ray telescopes, in particular in galaxies lacking an absorbing interstellar medium. However, recent studies found very little total soft X-ray emission in gas-poor elliptical galaxies (Gilfanov & Bogdan 2010), and far too few sources (Di Stefano 2010), implying that no more than  $\sim 5\%$  of the SNe Ia in these systems formed according to the standard SD scenario.

Such a direct argument is very efficient in constraining populations of relatively high temperature white dwarfs accreting in the steady nuclear burning regime. It is, however, much less sensitive to lower temperature sources (below  $T_{eff} \sim 4 \cdot 10^5$  K), which may arise in the so-called accretion wind state of the SD scenario, wherein the photosphere of the WD inflates to dimensions significantly exceeding the white dwarf radius. This would shift the peak of the radiation from the soft X-ray to the extreme UV regime, with temperatures roughly around  $1 - 2 \cdot 10^5$  K (Hachisu, Kato & Nomoto 2010). The total column density towards any such source would easily obscure it, preventing the direct detection of this UV emission. However, its signature will be seen as a hard ionizing source.

In fact, with harder UV spectra than young O-stars, old horizontal-branch stars or post-asymptotic giant branch stars (pAGBs), the presence of a SD-progenitor population will dramatically change the character of the ionizing background of a galaxy, in particular in the absence of a central active nucleus or for regions sufficiently far from one. In turn, the hardness of the ionising background could be gauged in the presence of a diffuse ionised-gas medium, by measuring the strength of nebular emission that can only be powered by a far-UV background, e.g. the He II recombination line at 4686 Å (He II  $\lambda 4686$ ). The strength of this line is indeed predicted to be considerably boosted should SNe Ia originate from hot and luminous WD progenitors compared to

a situation where the ionizing background is dominated by old UV-bright stars (Woods & Gilfanov 2013).

Hence, in this paper, the aim is to examine whether a substantial population of steadily-accreting WDs with black-body temperatures around a few times  $10^5$  K is consistent with measurements for the strength of He II  $\lambda 4686$  emission from the diffuse ionized-gas of galaxies, which we will use as a gauge for the hardness of the ionizing background. In particular, we focus on galaxies with  $> 1$  Gyr old passively-evolving stellar populations (also referred to as “retired galaxies”) with no sign of active galactic nuclei (AGN). Such a selection excludes the contribution of young and hot stars or of an accreting supermassive black hole to the ionizing background, leaving us to consider only the presence of old UV-bright stars such as pAGB stars in addition to the possible impact of accreting WDs. Retired galaxies have been shown to often host substantial amounts of neutral gas largely confined to a disk-like planar distribution within their host galaxy (Serra et al. 2012). This neutral gas is accompanied by extended regions of lowly-ionized gas (e.g., Sarzi et al. 2006), the emission of which has long been thought to be powered by a diffuse ionizing background supplied by stellar populations (Binette et al. 1994).

Retired galaxies are therefore an ideal laboratory to check whether a substantial accreting WD population of SN Ia progenitors exists. Yet, even though the presence of such hot sources would substantially boost the observed He II  $\lambda 4686$  emission from the interstellar medium of retired galaxies, the recombination lines remain intrinsically faint and their detection very challenging. For instance, in the case where pAGB stars are the only sources of He II -ionizing photons, the strength of the He II  $\lambda 4686$ -line is predicted to require a signal-to-noise (S/N) ratio in the stellar continuum  $> 500$  to be detected (Woods & Gilfanov 2013). This high-quality requirement contributes not only to explain why to date there is no reported detection of He II-emission in retired galaxies, but also sets the bar for the accuracy needed for our experiment if we wish to recognize an increase in the He II strength due to the presence of accreting WDs.

To achieve the required data quality, we will draw from the great wealth of optical spectra of nearby galaxies available in the Sloan Digital Sky Survey (SDSS, York et al. 2000) and co-add a large number of spectra of passively evolving systems with no sign of recent star formation or AGN activity, but for which we can detect the same kind of low-ionization nebular emission that is generally observed in nearby early-type galaxies. Such an emission is indeed always extended and has been shown to be consistent with the weak emission found in the SDSS spectra of retired galaxies, which cover most of the optical regions of these objects (Sarzi et al. 2010).

This paper is organized as follows. The data sample selection is described in Section 2. The technique used for stacking galaxy spectra and the method for estimating emission lines are described in Section 3. The derived He II  $\lambda 4686$  emission is presented Section 4 and compared to modelled predictions for the SD scenario in Section 5. Concluding remarks are given in Section 6.

**Table 1.** The corresponding number of galaxies left after applying each of the different sample cuts, starting from the full SDSS DR7 catalogue.

Selection	N
DR7	927 552
Redshift cut	305 598
WHAN cut	13 875
RSF cut I (PCA)	11 593
RSF cut II (NUV- <i>r</i> )	4 061

## 2 DATA SAMPLE

The sample used in this study is selected from the SDSS-II data release 7 (DR7 Abazajian et al. 2009). The SDSS has obtained imaging (*ugriz*; Fukugita et al. 1996) and spectroscopy for more than 930 000 galaxies. This was achieved with the multi-object spectrograph (Smee et al. 2013), fed with light from fibres with a fixed diameter of 3'', and wide-field CCD camera (Gunn et al. 1998) on the SDSS 2.5 m telescope (York et al. 2000; Gunn et al. 2006) at the Apache Point Observatory. Starting from the full DR7 sample we apply a number of selection criteria described below. The numbers of the samples after applying each cut are presented in Table 1.

### 2.1 Redshift and WHAN selection

For the stacking procedure we want to avoid galaxies for which the fixed SDSS aperture only covers the nuclear regions. Hence, we apply a lower redshift limit of  $z > 0.04$ , such that all spectra cover the galaxy stellar light within a diameter  $>\sim 2.5$  kpc. While the wavelength coverage of the SDSS spectra allows for  $\text{H}\alpha$  to be detected up to  $z \sim 0.4$ , we do also apply an upper redshift limit of  $z < 0.1$ , above which the signal-to-noise (S/N) of the SDSS spectra decreases fast. There are  $\sim 306 000$  SDSS DR7 galaxies for the adopted redshift range of  $0.04 < z < 0.1$  (“Redshift cut” in Table 1).

Most critically, we want to select gas rich galaxies where the ionizing photon field is not powered by young OB-stars or accreting black holes. For this purpose we use the combination of  $\text{H}\alpha$  line flux and  $\text{H}\alpha/\text{[N II]} \lambda 6584$  line ratio, the so called WHAN diagram (Cid Fernandes et al. 2011), to discriminate between objects where the nebular emission is powered by star-formation, an active galactic nucleus (AGN) or old and UV-bright stellar sources such as pAGB stars. Galaxies with detected  $\text{H}\alpha$  and  $\text{[N II]} \lambda 6584$  emission were selected from the OSSY value-added SDSS catalogue (Oh et al. 2011). In this process objects with robust emission-line fits of  $\text{H}\alpha$  and  $\text{[N II]} \lambda 6584$ , i.e. with an amplitude-over-noise (A/N) ratio  $> 3$  for both lines, were selected. Furthermore, objects with telluric emission contaminating these lines were excluded (Oh et al. 2011). The WHAN-diagram for the selection of galaxies with detected  $\text{H}\alpha$  and  $\text{[N II]} \lambda 6584$  lines is shown in Fig. 1. Region “SF” covers star-forming galaxies, region “AGN” galaxies hosting AGNs and region “Retired Galaxies” where old UV-bright stellar sources alone should suffice to ionize the interstellar medium (Cid Fernandes et al. 2011). The selection-limit of the latter region is  $\log \text{EW}_{\text{H}\alpha} < 0.48$ . We adopt a more conservative limit of  $\log \text{EW}_{\text{H}\alpha} = 0.3$  to minimize the AGN con-

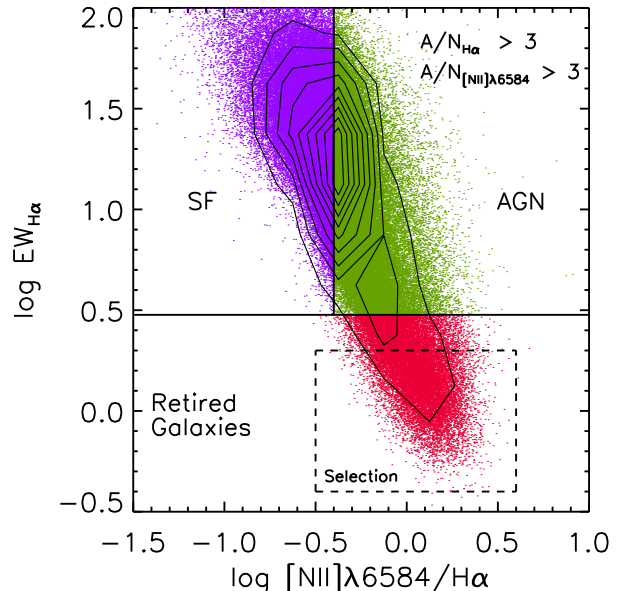


**Figure 1.** The WHAN-diagram (Cid Fernandes et al. 2011),  $[\text{N II}] \lambda 6584/\text{H}\alpha$  line ratio versus the strength of  $\text{H}\alpha$  (quantified by its equivalent width), for SDSS galaxies with detected  $\text{H}\alpha$  and  $[\text{N II}] \lambda 6584$  emission, i.e. for which the  $A/N > 3$  for both lines. The regions defined by the solid lines include galaxies with ionizing UV-radiation dominated by young stars in star-forming (SF) regions (top left), an AGN (top right) or UV-bright sources in old stellar populations (bottom). The dashed box represents our selection of old, so-called retired galaxies.

tamination. This selection criterion, indicated by the dashed box in Fig. 1, produces a sample of 13 875 galaxies (“WHAN cut” in Table 1).

### 2.2 Selecting galaxies without star formation in the last Gyr

In the last selection step, we discard galaxies hosting a significant fraction of stars younger than 1 Gyr. For this purpose we use the principal component analysis (PCA) technique of Chen et al. (2012) that is based on the work of Wild et al. (2007). The PCA method reproduces galaxy spectra by a set of orthogonal principal components. These components represent spectral features including the 4000 Å break and Balmer absorption lines that are very sensitive to the presence of young stars. Important for this work, the PCA technique of Chen et al. (2012) exploits these features to trace the fraction of stars formed in the last Gyr. After running a PCA on the individual galaxy spectra, we exclude objects where more than one per cent of the stellar mass has formed in a recent star formation (RSF) episode in the last Gyr, resulting in a final sample of 11 593 galaxies (“RSF cut I (PCA)” in Table 1).

Complementary to the PCA technique, we separately exclude galaxies with recent star formation by combining near ultra-violet (NUV) photometry with SDSS *r* band magnitudes. For this purpose, we cross-match the selected SDSS sample, i.e. WHAN cut (see Table 1), with the galaxy evolution explorer (GALEX) data base (Martin et al. 2005) to retrieve NUV magnitudes for the individual galaxies. We

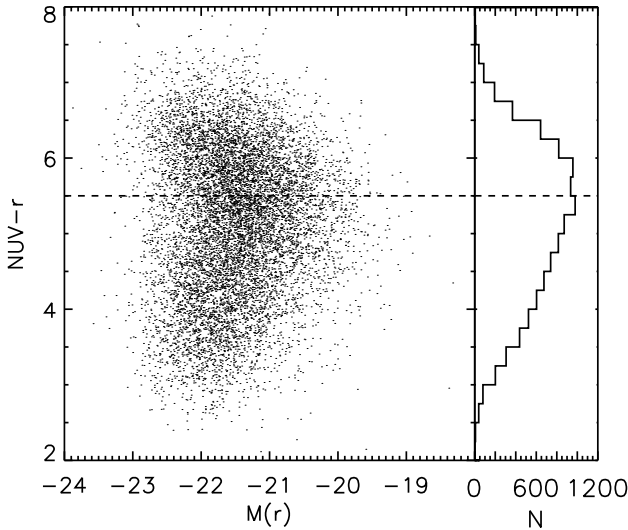


**Figure 2.** Left panel: NUV-*r* colour as a function of absolute *r* band magnitude  $M(r)$  for the 10 406 WHAN selected galaxies with available GALEX NUV magnitudes. The dashed line represents the limit from Kaviraj (2007), for which galaxies falling in the region below have experienced star formation in the last Gyr. Right panel: Distribution of NUV-*r* colours for the same sample selection as above.

find available GALEX photometry for 75 per cent of the selected galaxies, i.e. for 10 406 out of the 13 875 objects (see Section 2.1) in our sample. Objects with any star formation in the last Gyr typically have NUV-*r* colours  $< 5.5$  (Kaviraj 2007). The 10 406 galaxies with available NUV magnitudes are shown in Fig. 2 for NUV-*r* colour versus absolute *r* band magnitude  $M(r)$  (left hand panel), where the dashed line indicates the limit from Kaviraj (2007). The right hand panel shows the histogram of NUV-*r* colour. This selection criterion is more conservative than using the PCA approach and leaves a final sample of 4 061 galaxies (“RSF cut II (NUV-*r*)” in Table 1). This smaller sample leaves less freedom in the co-addition and analysis of stacked spectra, but it is a good complement to test and confirm the results of the PCA selected sample.

### 2.3 Stellar age estimates and age grouping

In order to better constrain the predictions concerning the strength of the He II  $\lambda 4686$  line within the single-degenerate progenitor model for SN Ia, we divided our final galaxy samples (“RSF cut I (PCA)” and “RSF cut II (NUV-*r*)” in Table 1) into several bins of average stellar population age. The ages are derived, together with stellar metallicity and element abundance ratios ( $O/Fe$ ,  $Mg/Fe$ ,  $C/Fe$ ,  $N/Fe$ ,  $Ca/Fe$  and  $Ti/Fe$ ), using the technique from Johansson et al. (2012) which is based on absorption line indices. This technique was developed to break the degeneracy, exhibited by the integrated light of stellar populations, of stellar age with both stellar metallicity and element abundance ratios. Moreover, absorption line indices are not prone to extinction uncertainties due to their narrow wavelength definitions. The reader is referred to Johansson et al. (2012) for details of the method, while only a brief description is given here.

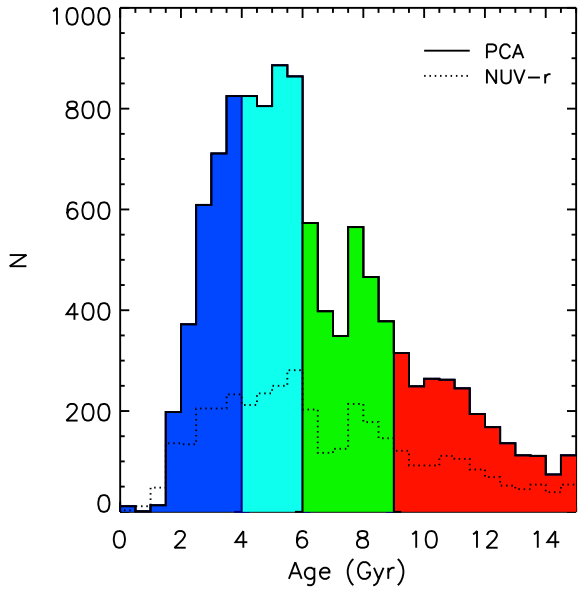


**Figure 3.** Distribution for the luminosity-weighted mean stellar age of our selected sample of retired galaxies. The coloured sub-histograms represent our four adopted age bins, which contain a similar number of galaxies. The solid and dashed histograms represent the samples where galaxies with star formation in the last Gyr have been discarded using the PCA and NUV-*r* criteria (see text), respectively, as indicated by the labels in the upper right corner.

The main working algorithm of the method is the fitting of observed and modelled absorption line indices using a  $\chi^2$ -minimization routine. The indices are defined for 25 prominent absorption features in the optical, known as the Lick indices (Worley et al. 1994). The observed Lick indices are taken from the OSSY data base. Following standard procedures, these indices were measured on emission line corrected absorption spectra downgraded to the Lick/IDS resolution (Worley & Ottaviani 1997), and finally corrected for velocity dispersion broadening. The  $\chi^2$ -minimization routine adjusts the stellar population models of Lick indices from Thomas, Maraston & Johansson (2011, TMJ) in order to match the observed values. This is done through a number of steps in order to carefully account for the sensitivity to the full range of element abundance ratios of the Lick indices. At each step a new set of models is used that is a perturbation of the previous best-fitting model. The best-fitting model at the final step, i.e. when the  $\chi^2$  is not improved by more than 1 per cent, determines the stellar population parameters of the galaxy spectrum examined.

This routine is run for all individual galaxy spectra included in the final selections (“RSF cut I (PCA)” and ‘RSF cut II (NUV-*r*)’ in Table 1). The age distributions for the selections are shown in Fig. 3, where the solid histogram shows the distribution for the PCA selection and the dotted histogram shows the NUV-*r* selected analogue. The former distribution is divided in bins containing at least  $\sim 2000$  objects, as shown by the coloured sub-histograms. This is the number needed to reach a desired S/N of  $\sim 500$  of the stacked spectra for the detection of the He II  $\lambda 4686$  lines with as low predicted equivalent width values as  $\sim 0.05$  Å, according to Woods & Gilfanov (2013), estimated using the

**Table 2.** Salient features of each of the co-added spectra analysed in this work. The columns give the age range of the galaxies in each group (col. 1), method for discarding galaxies with stars formed in the last Gyr (col. 2), number of spectra in each group (col. 3) and resulting S/N for the stacked spectra (col. 4) computed using the propagation of the formal SDSS uncertainties (see Section 3.1).

Stack		N	S/N
All ages	PCA	11593	1751
<4 Gyr	PCA	2740	882
4–6 Gyr	PCA	3380	1044
6–9 Gyr	PCA	2729	1000
>9 Gyr	PCA	2744	1018
<6 Gyr	NUV- <i>r</i>	1953	829
>6 Gyr	NUV- <i>r</i>	2108	951

mean S/N of the SDSS spectra of  $\sim 15$ . Hence, the sample is divided into four age bins ( $< 4$  Gyr,  $4 - 6$  Gyr,  $6 - 9$  Gyr and  $> 9$  Gyr), each with a number of objects greater than 2000. These numbers are presented in Table 2 for each age bin together with the resulting S/N after stacking all individual spectra (see Section 3.1). The more conservative cut using the NUV-*r* colour allows for a division into two age bins ( $< 6$  Gyr and  $> 6$  Gyr), in order to have  $\sim 2000$  galaxies in each bin.

### 3 CO-ADDITION AND ANALYSIS OF THE RESULTING STACKED SPECTRA

#### 3.1 Stacking technique

Prior to stacking the spectra of the different sample selections, a few corrections are applied to the individual spectra:

- (i) The additional flux calibration of Yan (2011) is applied to correct for small-scale fluctuations.
- (ii) The spectra are de-reddened for Galactic extinction following the extinction curve of diffuse gas from O'Donnell (1994) for an  $R_v$  value of 3.1, and using the Galactic E(B-V) values from the maps of Schlegel, Finkbeiner & Davis (1998).
- (iii) The spectra are brought to rest-frame wavelengths and to a common wavelength grid.

After applying these corrections, the spectra of each sample selection are co-added in emitted flux to produce high S/N stacked spectra. We have also co-added the spectra in emitted luminosity and after normalizing them using the average flux in a wavelength window of  $\pm 250$  Å around 5000 Å. The results from using the different stacking techniques are very similar, i.e. for the studied emission line ratio He II  $\lambda 4686/\text{H}\beta$  (see Section 4) the difference is less than the  $1\sigma$ -errors. Hence, the results are not biased by the adopted stacking technique. During the stacking process, the statistical error arrays associated with each SDSS spectrum are co-added in quadrature. Computed using this propagation of the formal SDSS uncertainties, the mean S/N around 5000 Å ( $\pm 250$  Å) for all sub-samples are presented in Table 2 (col. 4) and vary between  $\sim 830$  and  $\sim 1040$  for the different age bins and reach a value of  $\sim 1750$  for stacking all galaxies selected with the PCA criterion (see Section 2.2).

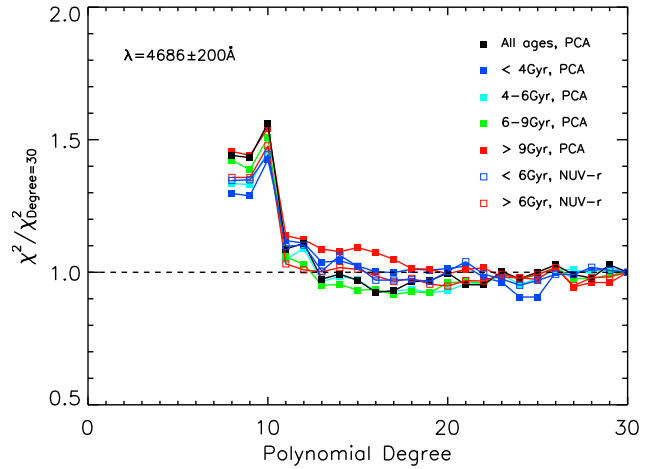


**Figure 4.** The  $\chi^2$  value derived in a wavelength window  $\pm 200$  Å around 4686 Å as a function of the polynomial degree used for adjusting the stellar templates in the SED fitting procedure (see text), normalized to the  $\chi^2$  value using a polynomial degree of 30. The various colours represent the different age bins used for stacking spectra as given by the labels.

It should be noted that redshift uncertainties have not been accounted for in the stacking process. Instead, we have verified, through Monte Carlo simulations, that including these uncertainties, the flux density errors of the stacked spectra increase by  $\sim 10$  per cent only. We also note that the S/N values in Table 2 are presented for illustrative purposes and should be considered approximations for characterizing the quality of the stacked spectra. Using the residual noise level of the fits (see Section 3.2) as an additional way of estimating the S/N ratios, we find similar but typically lower values by  $\sim 10 - 30$  % for the different age bins.

#### 3.2 Emission line fitting

With the aim of measuring emission lines we adopt the fitting code GANDALF (Sarzi et al. 2006). A brief description of this code is given here, while the reader is referred to Sarzi et al. (2006) for a detailed description. The goal of GANDALF is the separation of emission and absorption spectra of composite galaxy spectra. In the first step, the emission lines of the wavelength range under consideration are masked and the PPXF code (Cappellari & Emsellem 2004) is used for measuring kinematic broadening of the absorption spectrum with a set of best-fitting stellar templates. The emission line mask is then lifted and with the stellar kinematics fixed, GANDALF reassess the stellar continuum by simultaneously fitting a number of Gaussian emission line templates consisting of both re-combination and forbidden lines.

As stellar templates we adopt the full medium-resolution Isaac Newton telescope library (MILES, Sánchez-Blázquez et al. 2006). This library consists of observed spectra for 985 solar neighbourhood stars. This is the stellar library with the largest parameter coverage in the literature and, hence, allows us to achieve a very precise fit to the stellar continuum of the stacked spectra. The precision of the fit is significantly higher compared to using

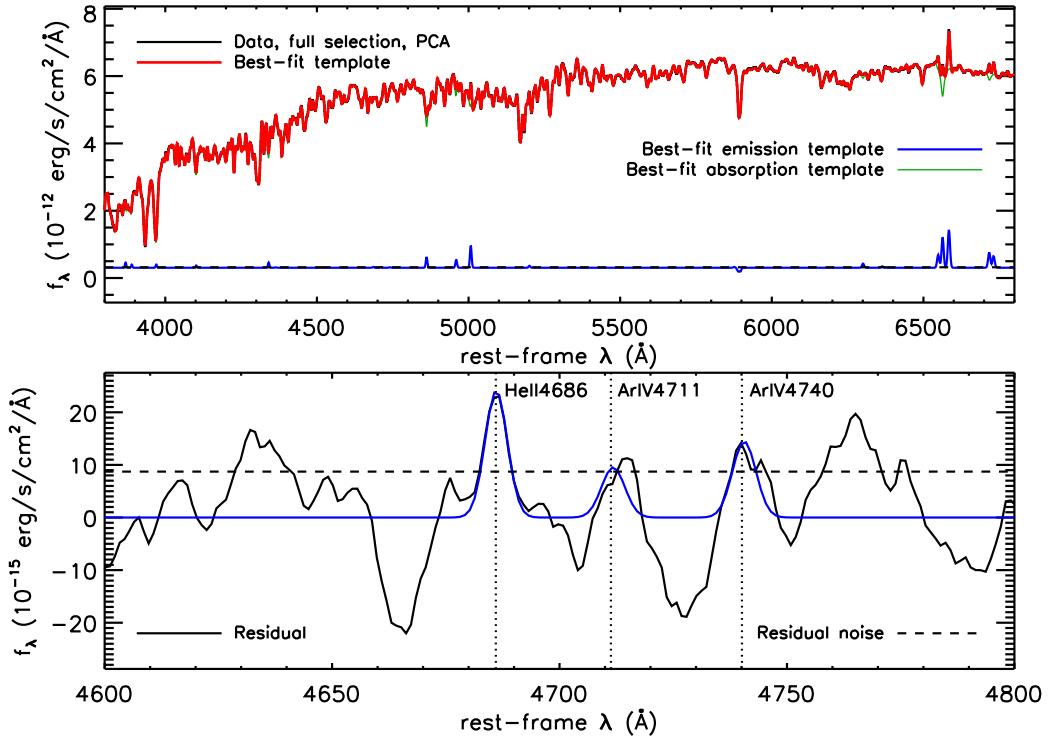


**Figure 5.** Data and model of stacked spectrum. Upper panel: total spectrum obtained by co-adding the spectra of all galaxies in our sample of quiescent objects (11593 galaxies) and selected using the PCA criterion (see Section 2), together with our best-fitting model (red line). The stellar component of this model is shown by the thin green line, whereas our best-fitting nebular spectrum is shown in blue. Lower panel: difference between the stacked spectrum and best-fitting stellar model around the position of the He II  $\lambda 4686$  line (black solid line), together with our best-fitting emission-line model (blue line). The dashed horizontal line shows the level of noise in the residuals (standard deviation) of the overall fit to the data in a wavelength region  $\pm 200$  Å around 4686 Å. In the 4600–4800 Å wavelength range, beside He II  $\lambda 4686$ , we also fit for the [Ar IV] lines at 4711 and 4740 Å. The position of all lines is indicated by dotted vertical lines, with labels for their name. In this case, the ratio between the Gaussian model amplitude and the level of noise in the residuals, A/N, which relates to the detection level of the lines, is 2.8 for the He II  $\lambda 4686$ -line.

stellar population models as templates (Cappellari et al. 2007; Sarzi et al. 2010).

The MILES library has a fixed instrumental full width half maximum (FWHM) resolution  $\Delta\lambda \sim 2.5$  Å (Beifiori et al. 2011), while the SDSS resolution is fixed at  $R \sim 2000$  which corresponds to a FWHM  $\Delta\lambda \sim 2.5$  Å at 5000 Å. Even though the resolutions are close, the MILES resolution is slightly higher at wavelengths longer than 5000 Å and vice versa. Hence, we degrade both the SDSS and MILES spectra to match each other prior to running GANDALF.

We perform our GANDALF fitting in the wavelength window between 3800 Å and 6800 Å, which includes many prominent absorption features useful for constraining the best-fitting set of stellar templates, as well as a wide range of important emission lines. This wavelength range specifically covers the strong H $\alpha$  and [N II] $\lambda\lambda 6584$  lines, which are useful for constraining the position and Gaussian width of weaker emission lines such as He II  $\lambda 4686$  and H $\beta$ . In particular, we tied the kinematics of all forbidden lines, such as the [O III] $\lambda\lambda 4959, 5007$  doublet, to the [N II] $\lambda 6584$  kinematics, whereas all recombination lines were tied to H $\alpha$ .

When running PPXF and GANDALF we adjust the fit of the templates to the stellar continuum using multiplicative

polynomials up to a relatively high order, 15, capable of affecting the continuum shape at a 200 Å level. Using a simple reddening law instead of polynomials would lead to considerably worse fits, most likely owing to residual uncertainties in the flux calibration of both object and template spectra. In Appendix A we evaluate the effect of adjusting the stellar continuum using multiplicative polynomials and conclude that for the great part the polynomial correction accounts for the effects of reddening by dust, with higher order terms being needed for additional weak corrections on small scales (see Fig. A8).

The polynomial degree was chosen to maximize the quality of the fit around the He II  $\lambda 4686$  ( $\pm 200$  Å) and we find that the  $\chi^2$  does not generally decrease for degrees greater than 15. This is shown in Fig. 4 where the  $\chi^2$  values, normalized to the  $\chi^2$  value for a degree of 30, are presented as a function of polynomial degree. The  $\chi^2$ -ratio generally flattens out at a degree of 15, hence, there is no gain in using a higher degree for detecting the He II  $\lambda 4686$  line. From now on, only results for adopting a degree of 15 are presented and discussed. Once an emission line is fit by GANDALF, we trace its level of detection through the A/N ratio between the Gaussian model peak amplitude and the level of noise in the residuals of the global fit, which we measure within

**Table 3.** Age range and selection criterion of the galaxies in each group (col. 1-2), cols. 3-5 list the A/N ratio corresponding to our fit for the He II  $\lambda 4686$ , H $\beta$  and [O III]  $\lambda 5007$  lines, respectively, whereas cols. 6 and 7 list the values for the He II  $\lambda 4686$ /H $\beta$  and [O III]  $\lambda 5007$ /H $\beta$  line ratios. Col. 8 gives the derived average stellar population age.

Stack			A/N He II H $\beta$	[O III]	He II /H $\beta$	[O III ]/H $\beta$	Age (Gyr)
All	PCA	2.8	32.2	53.4	0.073±0.021	2.24±0.06	4.7
<4 Gyr	PCA	2.7	32.6	51.9	0.075±0.023	1.95±0.06	2.8
4-6 Gyr	PCA	3.0	30.9	53.6	0.089±0.023	2.22±0.07	4.9
6-9 Gyr	PCA	2.6	28.0	47.8	0.087±0.026	2.31±0.08	6.6
>9 Gyr	PCA	2.6	23.8	39.9	0.103±0.029	2.32±0.09	10.7
<6 Gyr	NUV-r	2.7	28.5	52.4	0.088±0.023	2.28±0.07	3.0
>6 Gyr	NUV-r	2.6	23.8	40.1	0.101±0.026	2.31±0.09	8.7

a  $\pm 200$  Å-wide wavelength window around the line of interest. Hence, from now on we refer noise to the residual noise, instead of the propagation of the formal SDSS uncertainties used as a measure of the noise in Section 3.1. Generally, a value of A/N greater than 3 is considered sufficient to grant detection of a line for which the kinematics has been held fixed (Sarzi et al. 2006). However, in Section 4.1, we further investigate the detection level associated with any given A/N value in the case of the He II  $\lambda 4686$  line.

The ability to estimate the amplitude of the lines, which depends on the residual noise level, dominates the error of the line fluxes (Sarzi et al. 2006). Statistical errors are not the only contribution to the residual noise level, but systematic uncertainties, or template mismatch, will contribute as well. Hence, to properly estimate the amplitude errors the statistical errors are scaled to get a  $\chi^2 \sim 1$  for the overall fit (Sarzi et al. 2005).

As already mentioned, for the adopted wavelength range we fit a large number of emission lines. However, in this paper we focus on the detection of the He II  $\lambda 4686$  line. In addition to this line, we will also use the results for H $\beta$  and [O III]  $\lambda 5007$  (see Section 5) in order to constrain the ionization state of the gas. All other detected optical lines will be discussed in a companion paper (Johansson et al., in preparation).

## 4 STACKING RESULTS

In this section, we present the results for the lines He II  $\lambda 4686$ , H $\beta$  and [O III]  $\lambda 5007$  from the SED fitting of the stacked spectra using GANDALF. In particular, we assess the confidence level of the detection of the weak He II  $\lambda 4686$  line. Furthermore, we derive the average stellar population age of the emission corrected stacked spectra.

### 4.1 Emission lines

The spectrum obtained when stacking all selected galaxies using the PCA criterion (see Section 2.2) is presented in Fig. 5 (upper panel) together with our best-fitting model. The stacked spectrum is matched by the best-fit template to a very high precision and a range of prominent emission lines are apparent. Corresponding figures for the rest of the stacked spectra are presented in Appendix A (Fig. A1-A6), together with a zoom-in on the fit around He II  $\lambda 4686$ , H $\beta$  and [O III]  $\lambda 5007$  (Fig. A7). The lower panel of Fig. 5 shows

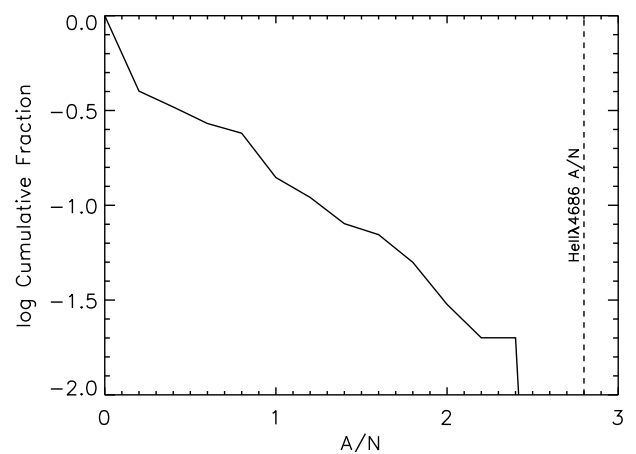


**Figure 6.** The cumulative fraction of A/N values obtained when asking GANDALF to fit non-existing emission lines at 100 randomly-generated spectral positions around the He II  $\lambda 4686$  line ( $\pm 200$  Å). This gives the probability of finding a line with a specific A/N value, or above, just by chance. This test was run on the stacked spectrum obtained from our entire sample using the PCA criterion (11 593, see Section 2 and Table 1), and while imposing on GANDALF to look for fake lines with the same Gaussian line profile as observed for the [N II]  $\lambda 6548, \lambda 6584$  lines. We find similar probability distributions for all stacked spectra of the different age bins, as well as when repeating this experiment over different wavelength ranges (e.g. between 4800 – 5200 Å).

the difference between the stacked spectrum and best-fitting stellar template, together with the best-fitting emission-line model around the position of He II  $\lambda 4686$ . A positive feature is clearly visible at the location of the He II  $\lambda 4686$  line, which is well matched while adopting the same Gaussian profile as used when fitting the much stronger [N II] emission at 6584 Å. Most of the other features in the residuals of our stellar fit can be explained in light of the limitations of our adopted stellar templates (see Section 3.2). For instance, the strong negative feature at 4668 Å corresponds to a C<sub>2</sub>-absorption feature, which is not perfectly matched by the stellar model because the templates cannot account for the super-solar Carbon abundance that is observed in massive galaxies (Johansson et al. 2012).

Table 3 lists the A/N values for the derived He II  $\lambda 4686$ , H $\beta$  and [O III]  $\lambda 5007$  lines (cols. 3-5) for each stacked spectrum. In the comparison with modelled emission line predictions for the SD scenario we focus on emission line ratios

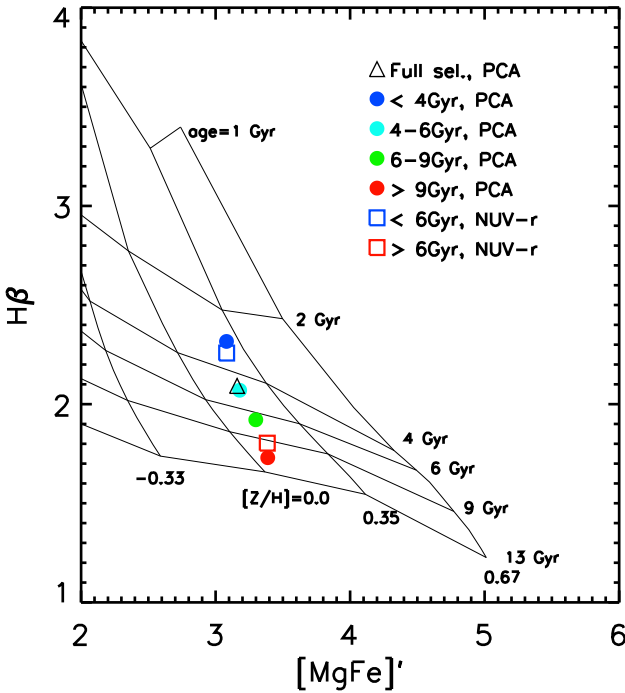


**Figure 7.** Diagnostic diagram for the absorption lines indices  $H\beta$  as a function of  $[MgFe]'$  (Thomas et al. 2003), both known to be insensitive to  $[\alpha/Fe]$ -variations. Coloured points are indices derived on the emission line subtracted, stacked spectra according to the labels. The black grids are stellar population models (Thomas et al. 2011) of varying age and metallicity as given by the labels and for  $[\alpha/Fe]=0.3$ . This shows that our division of individual galaxies into age-bins was successful.

instead of individual line fluxes (see Section 5). Hence, the value of the  $\text{He II } \lambda 4686/\text{H}\beta$  flux ratio is presented in Table 3 (col. 6), together with the  $[\text{O III}]\lambda 5007/\text{H}\beta$  line ratio (col. 7) used for constraining the ionization parameter (see Section 5). The strong  $[\text{O III}]\lambda 5007$  and  $\text{H}\beta$  lines are always undoubtedly detected with A/N ratios greater than 40 and 23, respectively. The A/N ratios of the  $\text{He II } \lambda 4686$  line instead falls in the range 2.6–3.0. As mentioned above, the residual noise determining the A/N value of this weak line is dominated by systematics, i.e. the ability of the stellar templates to recover the stacked absorption spectra. Thus, in the following section we assess the confidence level of the detection of the  $\text{He II } \lambda 4686$  line. At this point, we note that for all age bins we appear to find consistently low values (less than 0.1) for the  $\text{He II } \lambda 4686/\text{H}\beta$  ratio. We also note that the  $\text{He II } \lambda 4686$  flux appears to be slightly overestimated in the oldest age bin (see Appendix A for more details).

#### 4.2 The A/N ratio as a tracer for the detection level of $\text{He II } \lambda 4686$

To further understand the connection between any measured value of the A/N ratio and the level of detection for the  $\text{He II } \lambda 4686$  line, we have used the GANDALF procedure to look for emission lines with the same line profile of the strong  $[\text{N II}]\lambda\lambda 6548, 6584$  lines in spectral regions where no significant emission is known to exist. More specifically, by repeating this experiment 100 times at random spectral positions

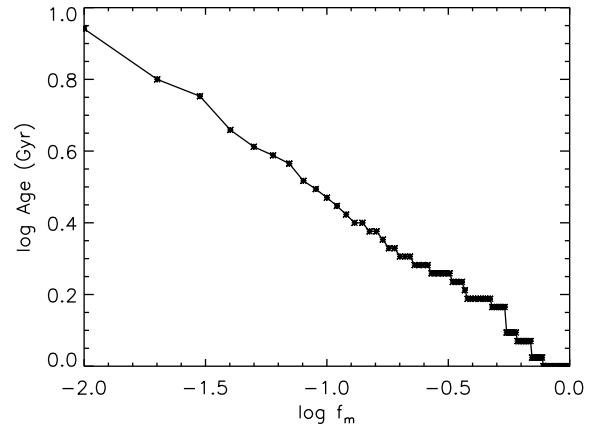


**Figure 8.** The luminosity-weighted age of composite stellar populations consisting of the mass fractions  $f_m$  of a 1 Gyr old SSP and  $1 - f_m$  of a 10 Gyr old SSP. The composite stellar populations were modelled using the spectra of SSP models from Bruzual & Charlot (2003) and the luminosity weighted ages were derived using absorption line indices as described in Section 2.3.

around the  $\text{He II } \lambda 4686$  line ( $\pm 200$  Å) we have assessed the probability of measuring any given A/N value just by chance with our fitting procedure. In fact, assuming that the fit to the stellar spectrum is not particularly worse around the position of the  $\text{He II } \lambda 4686$  line than right on it, this test implicitly accounts for spurious emission-line measurements (and corresponding A/N values) that would be due to our limited ability to fit the real stellar spectra of galaxies with our current set of stellar templates, resulting in GANDALF attempting to compensate for this problem by means of a Gaussian feature. The cumulative distribution for the fraction of A/N values returned by our fake emission-line fits during this test is shown in Fig. 6. The plotted distribution was derived from the stacked spectrum corresponding to our entire sample using the PCA criterion (see Section 2.2), and similar distributions are obtained also from the stacked spectra for each of our stellar-age subsamples. This is not surprising as all spectra are characterized by similar systematic patterns of residuals around 4686 Å (compare Fig. 5 with Fig. A1–A6). In the  $\text{He II } \lambda 4686$  spectral region, the distribution plotted in Fig. 6 indicates that there is less than 5% probability of finding an  $A/N \sim 2.0$  or above, and less than 1% probability for values equal or in excess of an  $A/N \sim 2.4$ .

The values of the A/N ratio for the derived  $\text{He II } \lambda 4686$  lines always fall in the range between 2.6 and 3.0 (Table 3). Given that there is less than 1% probability of measuring A/N values of 2.4 and above for the  $\text{He II } \lambda 4686$  line in our stacked spectra, this line is robustly detected for all groups of galaxies with different luminosity-weighted stellar ages.

#### 4.3 Stellar population ages

By subtracting the emission line spectra from the stacked galaxy spectra, we get clean absorption spectra for which we derive the Lick indices (see Section 2.3). Fig. 7 shows the classic  $H\beta$  versus  $[MgFe]'$  line-strength diagram (Thomas et al. 2003) for the Lick indices derived on the stacked spectra, and with the TMJ models overlaid with

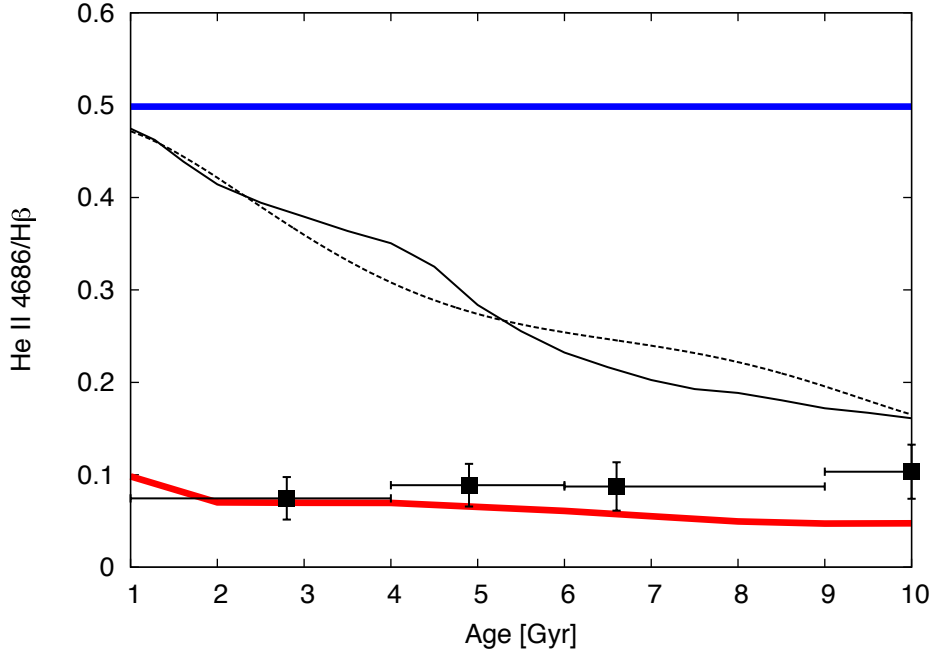


**Figure 9.** Comparison between observed values (filled squares, presented in Table 3) of the He II  $\lambda 4686/\text{H}\beta$  line ratio and our model predictions as a function of stellar age. The vertical and horizontal error-bars attached to our measurements represent the  $1\sigma$ -errors on the line ratio and the range of stellar ages encompassed by each of our subsamples, respectively. The red and blue thick lines show the predictions for ionization by single type of ionizing sources, either by pAGB stars or by accreting WDs in the SD scenario for SN Ia progenitors, respectively. The black solid line shows the predicted values for the He II  $\lambda 4686/\text{H}\beta$  ratio when both components are considered. In this case the spectrum of the stellar component (dominated by pAGB stars) was computed using the SSP models from Bruzual & Charlot (2003), whereas the luminosity of the SD SN Ia progenitors was computed using Eq. 1. In the latter, we assumed  $\Delta M_{\text{SD}} = 0.3M_{\odot}$ , a WD effective temperature of  $T_{\text{eff}} = 2 \cdot 10^5$  K and the age dependent SN Ia rate as given by the delay time distribution of Totani et al. (2008). To illustrate the impact of non-SSP stellar populations, the dashed black line shows the predictions for composite stellar populations combining 1 and 10 Gyr old SSPs (see text for details). Both single-age and two-burst models predict declining He II  $\lambda 4686/\text{H}\beta$  values, reflecting the cosmic decrease in the SN Ia rate. The observed values for the He II  $\lambda 4686/\text{H}\beta$  ratio are well below these models, appearing instead consistent with pAGBs being the only, or at least dominant, source of ionizing photons for the diffuse gas of quiescent galaxies.

ages and metallicities as given by the labels. This diagram is useful for visualizing stellar population parameters and the trend of the stacked spectra clearly follows that of the selected age bins. Furthermore, we apply our method for deriving stellar population parameters from observed Lick indices (Johansson et al. 2012, see Section 2.3) and the derived ages for each of the stacks are presented in Table 3 (col. 8). These measurements confirm that the division into age bins, based on the individual spectra, was successful.

Even though we have excluded objects with significant fractions of stars younger than a Gyr, our luminosity-weighted ages could still be biased by the presence of a small fraction of  $\sim 1$  to 2-Gyr-old populations. To account for this possibility, we compute the luminosity-weighted age of a composite stellar population consisting of the mass fraction  $f_m$  of a 1 Gyr old simple stellar population (SSP, i.e. single age and metallicity) superimposed on the fraction  $1 - f_m$  of a 10 Gyr old SSP. We adopt the SSP models from Bruzual & Charlot (2003), to be consistent with the model predictions of Woods & Gilfanov (2013), with metallicities of  $2.5Z_{\odot}$  and  $Z_{\odot}$  for the young and old components, respectively. Instead using the models from Maraston & Strömbäck (2011) gives a very similar result. The luminosity-weighted ages of the composite populations are determined from absorption line indices as described

in Section 2.3. The resulting dependence of the luminosity-weighted age on the mass fraction  $f_m$  of the 1 Gyr old SSP is shown in Fig. 8. This dependence will be used in the next section to derive predictions for the SD scenario for the different composite populations to estimate the range of possible strengths of the He II  $\lambda 4686$  line at a given stellar population age.

## 5 CONSTRAINTS ON THE SD SCENARIO

We now compare our emission-line results with the predictions of the photoionization models from Woods & Gilfanov (2013, we refer the reader to this paper for details of the models) that include possible SD progenitors of SN Ia. In particular, we focus on predicted values of the He II  $\lambda 4686/\text{H}\beta$  line ratio. This quantity remains as sensitive to the hardness of ionizing radiation as the He II  $\lambda 4686$  line itself, but does not depend on assumptions regarding dust extinction or the fraction of ionizing photons that is intercepted by the interstellar medium. It does depend on the ratio of the ionizing photon flux to the gas density in units of the speed of light (per Hydrogen atom, the so-called ionization-parameter  $U$ ). This is constrained by the observed  $[\text{O III}]\lambda 5007/\text{H}\beta$  ratio (see Table 3) following

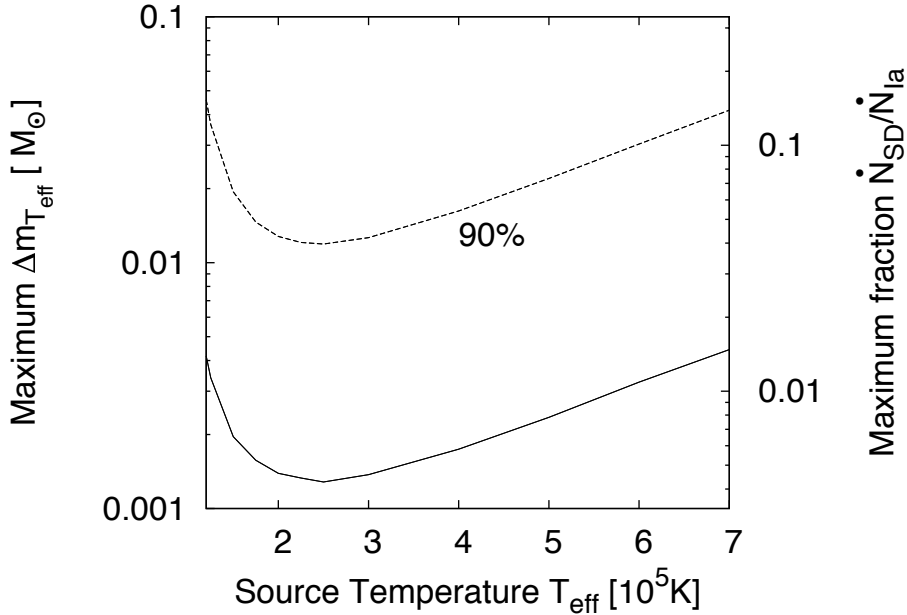


**Figure 10.** The maximum mass accreted by a typical white dwarf – successful SN Ia progenitor – as a function of its assumed effective temperature for the delay time of  $\approx 3$  Gyr, assuming that each SN Ia progenitor spends some time in the stable nuclear burning regime. The solid line shows the upper limit derived from the He II  $\lambda 4686/H\beta$  ratio measured in the co-added spectrum for the youngest galaxy sub-sample (1–4 Gyr). The dashed curve includes the statistical uncertainty in this ratio at the 90% confidence level. The right hand y-axis shows the maximum fraction of SN Ia which can be produced in the SD scenario, assuming that each SD-progenitor needs to accrete  $\Delta M_{SB} = 0.3 M_\odot$  of material.

Stasińska et al. (2008) and Yan & Blanton (2012). We find that in all age bins, the ratio  $[\text{O III}]\lambda 5007/\text{H}\beta$  is consistent with ionization by pAGB stars alone, with  $\log(U) \approx -3.5$  (see Johansson et al., in preparation). This then fixes the incident ionizing photon flux at the face of the nebula in our models (for a given mean density). Recall that the total luminosity of any SD progenitor population is, in an average sense, fixed by the SN Ia rate ( $\dot{N}_{SNIa}$ ) and the total amount of mass processed through steady burning ( $\Delta M_{SB}$ , c.f. Eq. 1). Therefore, varying the luminosity of the SD population through  $\Delta M_{SB}$  effectively varies the hardness of the ionizing radiation.

As a conservative estimate, we take  $\Delta M_{SB}$  in Eq. 1 to be equal to  $0.3 M_\odot$ , which corresponds to the difference of the critical Chandrasekhar mass ( $\approx 1.4 M_\odot$ ) and the maximum birth mass of a carbon-oxygen WD ( $\sim 1.1 M_\odot$ , Umeda et al. 1999). The observed He II  $\lambda 4686/\text{H}\beta$ -ratio as a function of stellar population age is compared with the results of photoionization calculations for SSPs and the SD scenario in Fig. 9. For the latter, we take a characteristic temperature of  $T_{\text{eff}} = 2 \cdot 10^5 K$ , corresponding to the particular scenario of a white dwarf embedded in an optically thick radiation driven wind (Hachisu et al. 1999). Note that this photospheric temperature is also consistent with the lower range of temperatures estimated for supersoft sources (e.g. SMC 3, Sturm et al. 2011). We produce photoionization models using both SSPs (solid line in Fig. 9) and composite populations (dashed line) for the ionizing emission. For the latter we use the fractions of 1 Gyr and 10 Gyr single burst populations derived in Section 4.3 over the entire 1–10 Gyr range. For luminosity-weighted ages above  $\sim 6$  Gyr, even a small

fraction of 1-Gyr-old stars in the composite models brings an overall higher rate of SN Ia and hence larger values of the predicted He II  $\lambda 4686/\text{H}\beta$  ratio than in the case of a pure old stellar population, whereas the converse holds for lower values of the luminosity-weighted age. The predictions shown in Fig. 9 for the single-age case and our particular composite models thus represent conservative upper and lower boundaries for the He II  $\lambda 4686/\text{H}\beta$  ratio that should bracket the case of less extreme, and more plausible, star-formation histories. The observed ratios are clearly well below those expected from models including a large population of accreting WDs. Notably, they are in agreement (within  $1\sigma$ ) with pABG stars being the sole ionizing source in retired galaxies. In Fig. 9 we only present the observed values for the PCA selection (see Section 2.2), which are in good agreement with the observed values for the NUV- $r$  selection (see Table 3).

Assuming that all WD progenitors of SN Ia go through a steady nuclear-burning phase, we can constrain the maximum amount of mass accreted at any photospheric temperatures above  $\sim 10^5 K$ <sup>1</sup> by requiring that our models do not conflict with the observed He II  $\lambda 4686/\text{H}\beta$ -ratio. This is shown in Fig. 10 (left axis) as a function of  $T_{\text{eff}}$ ,

<sup>1</sup> Note that in the wind models of Hachisu et al. (1999), photospheric temperatures below  $10^5 K$  require mass accretion rates in excess of  $10^{-5} M_\odot/\text{yr}$ , which would result in a prohibitively high mass loss rate and low mass accumulation efficiency for SN Ia progenitors. They are therefore irrelevant in the context of SN Ia progenitors in retired galaxies, because of the mass conservation considerations.

derived for the mean age ( $\approx 3$  Gyr, see Table 3) and observed He II  $\lambda 4686/\text{H}\beta$ -ratio of the youngest age-bin ( $< 4$  Gyr) where the SN Ia rate is high. This is derived accounting for the contribution from pAGBs. Taking the observed He II  $\lambda 4686/\text{H}\beta$ -ratio at face value, it may be concluded that the maximum mass accreted by a typical white dwarf – successful SN Ia progenitor – at photospheric temperatures of  $(1 - 7) \cdot 10^5$  K lies in the range  $\sim (1 - 4) \cdot 10^{-3} M_\odot$ . Note that the upper end of the temperature range is in fact more tightly constrained by X-ray observations (Gilfanov & Bogdan 2010). Accounting for the statistical errors on the He II  $\lambda 4686/\text{H}\beta$ -ratio at the 90 % confidence level, we obtain an upper limit of  $\sim 0.04 M_\odot$ , also falling far short of the minimum  $0.3 M_\odot$  required to trigger a SN Ia explosion.

Alternatively, we can estimate the maximum fraction of SN Ia originating from the SD-channel, again assuming that a white dwarf needs to accrete at least  $\Delta M_{\text{SB,min}} = 0.3 M_\odot$  in order to produce a supernova. This fraction is shown on the right-hand axis of Fig. 10 and does not exceed  $\sim 0.01$  for the observed He II  $\lambda 4686/\text{H}\beta$ -ratio. Accounting for the errors at the 90 % confidence level, we find an upper limit on the maximum fraction of SN Ia originating from the SD-channel of  $< 0.1$ . Note that the typical value of  $\Delta M_{\text{SB}}$  in the SD scenario should be larger than the assumed  $\Delta M_{\text{SB,min}} = 0.3 M_\odot$  resulting in an even more constraining upper limit.

## 6 CONCLUSIONS

We study nebular emission in passively evolving (“retired”) galaxies to constrain their populations of hot accreting WDs in the context of the SD scenario of SNe Ia. In the SD scenario, a WD accretes hydrogen-rich material from a companion star until sufficient mass has accumulated to trigger a thermonuclear explosion. During the accretion phase, the WD emits significant UV radiation, peaking in the extreme UV when the photosphere is significantly inflated (as in some SD models). The collective emission from a population of such objects will alter the ionization balance in the warm/cold component of the interstellar medium in retired galaxies where mainly pAGB stars are expected (weak) ionizing sources. Hence, the population of accreting WDs can be constrained by the strength of He II recombination lines.

For this purpose, we select galaxies from the SDSS with detected emission lines and where the ionizing background is not powered by AGNs or young stars in star forming regions. Furthermore, we select galaxies with stellar population ages  $> 1\text{Gyr}$  that have not experienced star formation episodes in the last Gyr. In total we select  $\sim 11500$  galaxies and their spectra are co-added in four bins of stellar population age resulting in  $> 2000$  galaxies in each bin, producing high quality stacked spectra with S/N values exceeding 800. For each stacked spectrum, we fit the SED in a wide wavelength range, 3800–6800 Å, where a number of emission lines reside including He II  $\lambda 4686$ , using the code GANDALF (Sarzi et al. 2006) and the observed stellar library MILES (Sánchez-Blázquez et al. 2006) as templates for the stellar continuum. In the fitting process, the kinematics and position of He II  $\lambda 4686$  are constrained by the strong [N II]  $\lambda\lambda 6548, 6584$  line doublet.

We extensively test the detection level of emission lines

in the wavelength region around 4686 Å and conclude that we, for the first time, detect the He II  $\lambda 4686$  line in retired galaxies. The line strengths of the stacked spectra in the four age bins are compared to the photoionization models from Woods & Gilfanov (2013) that include the ionizing contribution of accreting WDs in the SD scenario. For this comparison we focus on the He II  $\lambda 4686/\text{H}\beta$  line ratio, which is insensitive to dust reddening and the covering fraction of gas. We find that in all age bins the He II  $\lambda 4686/\text{H}\beta$  ratio is (much) smaller than that expected in the SD scenario. For galaxies in the youngest age bin ( $1\text{Gyr} < t_{\text{galaxy}} < 4\text{ Gyr}$ ), where the SN Ia rate is the highest for the considered range of stellar ages, the He II  $\lambda 4686$  line is more than 10 times weaker than predicted by the SD scenario. On the other hand, the observed He II  $\lambda 4686/\text{H}\beta$  line ratio is consistent with pAGB stars being the sole ionizing source in all age bins.

These results exclude the presence of any significant population of accreting WDs with photospheric temperatures in the  $\sim (1.5 - 7) \cdot 10^5$  K range. Thus, only a small fraction of less than  $\sim 5 - 10\%$  of SN Ia observed in retired galaxies could originate according to the classical version of the SD scenario. Furthermore, irrespectively of the particular scenario, should all WD progenitors of SN Ia go through the phase of steady nuclear burning with the photospheric temperature range  $\sim (1.5 - 7) \cdot 10^5$  K, they do not increase their mass by more than a few times  $10^{-2} M_\odot$  in this regime.

In this paper we have mainly focused on the He II  $\lambda 4686$  line, although we detect a large number of optical emission lines in the stacked spectra. A general discussion of observed optical lines in retired galaxies, as well as the inferred properties of the associated dust, will be presented in a subsequent paper (Johansson et al., in preparation).

## ACKNOWLEDGMENTS

We would like to thank an anonymous referee for useful comments that helped improve this paper. JJ would like to thank the Deutsche Forschungsgemeinschaft (DFG) for financial support. KO acknowledges support from the National Research Foundation of Korea (SRC Program No. 2010-0027910) and the DRC Grant of Korea Research Council of Fundamental Science and Technology (FY 2012).

## REFERENCES

- Abazajian K., et al., 2009, ApJS, 182, 543
- Beifiori A., Maraston C., Thomas D., Johansson J., 2011, A&A, 531, 109
- Binette L., Magris C. G., Stasińska G., Bruzual A. G., 1994, A&A, 292, 13
- Bruzual G., Charlot S., 2003, MNRAS, 344, 1000
- Cappellari M., Emsellem E., 2004, PASP, 116, 138
- Cappellari M., et al., 2007, MNRAS, 379, 418
- Chen Y.-M., et al., 2012, MNRAS, 421, 314
- Chomiuk L., 2013, Publ. Astron. Soc. Aust., 30, 46
- Di Stefano R., 2010, ApJ, 712, 728
- Cid Fernandes R., Stasińska G., Mateus A., Vale Asari N., 2011, MNRAS, 413, 1687

- Fukugita M., Ichikawa T., Gunn J.E., Doi M., Shimasaku K., Schneider D.P., 1996, AJ, 111, 1748
- Gilfanov M., Bogdán Á., 2010, Nature, 463, 924
- Graur O., et al., 2014, ApJ, 783, 28
- Gunn J. E., et al. 1998, AJ, 116, 3040
- Gunn J. E., et al. 2006, AJ, 131, 2332
- Hachisu I., Kato M., Nomoto K., 1999, ApJ, 522, 487
- Hachisu I., Kato M., 2001, ApJ, 558, 323
- Hachisu I., Kato M., Nomoto K., 2010, ApJ, 724, L212
- Johansson J., Thomas D., Maraston C., 2012, MNRAS, 421, 1908
- Kaviraj S., 2007, ApJS, 173, 619
- Maoz D., Mannucci F., Brandt T. D., 2012, MNRAS, 426, 3282
- Maraston C., Strömbäck G., 2011, MNRAS, 418, 2785
- Martin D. C. , et al., 2005, ApJ, 619, L1
- Nomoto K., Saio H., Kato M., Hachisu I., 2007, ApJ, 663, 1269
- O'Donnell J. E., 1994, ApJ, 422, 158
- Oh K., Sarzi M., Schawinski K., Sukyoung K. Yi, 2011, ApJS, 195, 13
- Perlmutter S., et al., 1999, ApJ, 517, 565
- Prialnik D., Kovetz A., 1995, ApJ, 445, 789
- Riess A. G., et al., 1998, AJ, 116, 1009
- Schlegel D. J., Finkbeiner D. P., Davis M., 1998, ApJ, 500, 525
- Sánchez-Blázquez P., et al., 2006, MNRAS, 371, 703
- Sarzi M., Rix H.-W., Shields J. C., Ho L. C., Barth A. J., Rudnick G., Filippenko A. V., Sargent W. L. W., 2005, ApJ, 628, 169
- Sarzi M., et al., 2006, MNRAS, 366, 1151
- Sarzi M., et al., 2010, MNRAS, 402, 2187
- Serra P., et al., 2012, MNRAS, 422, 1835
- Smee S. A., et al., 2013, AJ, 146, 32
- Stasińska G., et al., 2008, MNRAS, 391, L29
- Sturm R., et al., 2011, A&A, 529A, 152
- Thomas D., Maraston C., Bender R., 2003, MNRAS, 339, 897
- Thomas D., Maraston C., Johansson J., 2011, MNRAS, 412, 2183
- Totani T., Morokuma T., Oda T., Doi M., Yasuda N., 2008, PASJ, 60, 1327
- Umeda H., Nomoto K., Yamaoka H., Wanajo S., 1999, AJ, 513, 861
- van den Heuvel E. P. J. , Bhattacharya D., Nomoto K., Rappaport S. A., A&A, 262, 97
- Whelan J., Iben I. Jr., 1973, ApJ, 186, 1007
- Wild V., Kauffmann G., Heckman T., Charlot S., Lemson G., Brinchmann J., Reichard T., Pasquali A., 2007, MNRAS, 381, 543
- Woods T. E., Gilfanov M., 2013, MNRAS, 432, 1640
- Worthey G., Ottaviani D. L., 1997, ApJS, 111, 377
- Worthey G., Faber S. M., Gonzalez J. J., Burstein D., 1994, ApJS, 94, 687
- Yan R., 2011, AJ, 142, 153
- Yan R., Blanton M. R., 2012, ApJ, 747, 61
- York D., et al. 2000, AJ, 120, 1579

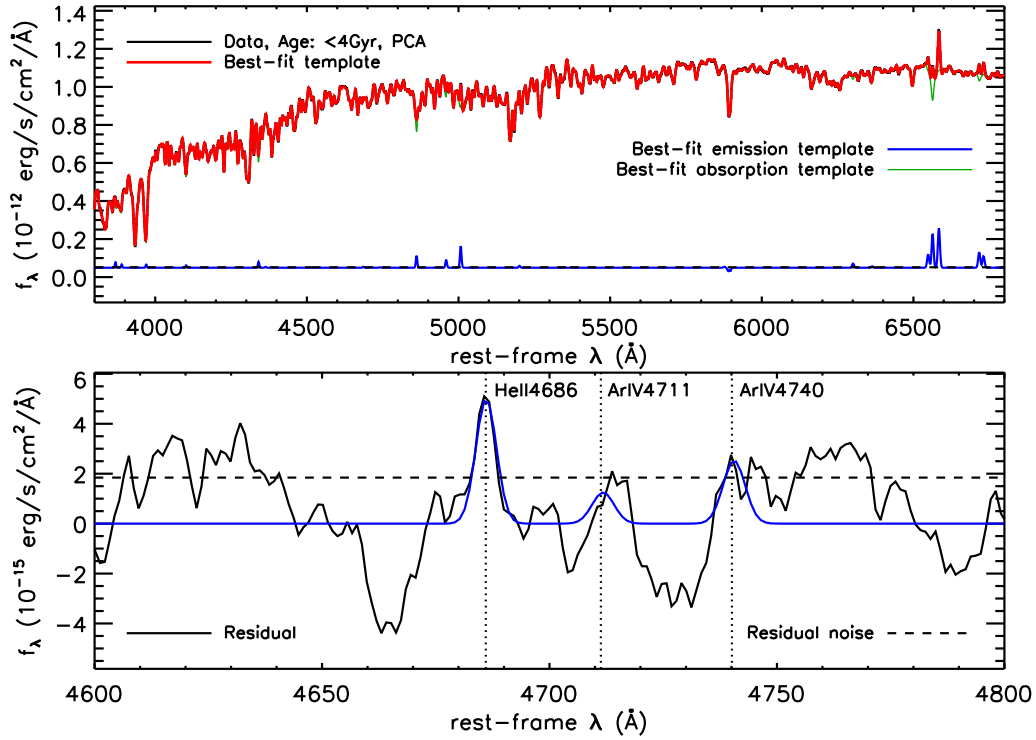


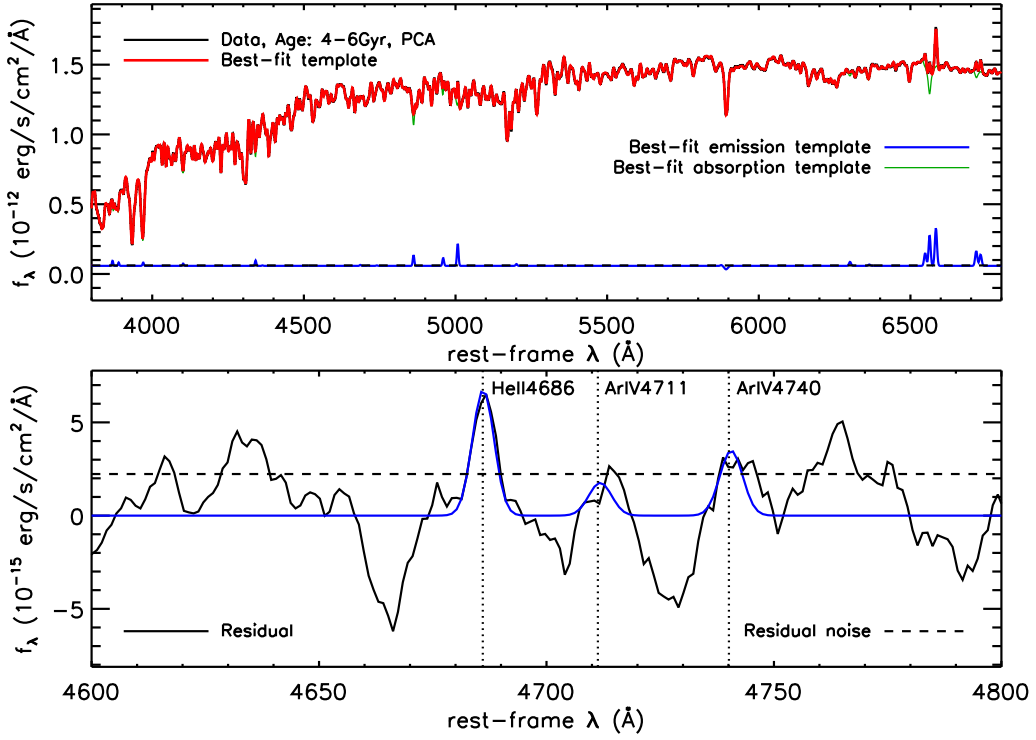
**Figure A1.** Data and model of stacked spectrum. Upper panel: total spectrum obtained by co-adding the spectra of all galaxies in our sample with luminosity-weighted mean stellar ages  $<4$  Gyr (2740 objects) and selected using the PCA criterion (see Section 2), together with our best-fitting model (red line). The stellar component of this model is shown by the thin green line, whereas our best-fitting nebular spectrum is shown in blue. Lower panel: difference between the stacked spectrum and best-fitting stellar model around the position of the He II  $\lambda 4686$  line (black solid line), together with our best-fitting emission-line model (blue line). The dashed horizontal line shows the level of noise in the residuals (standard deviation) of the overall fit to the data in a wavelength region  $\pm 200$  Å around 4686 Å. In the 4600–4800 Å wavelength range, beside He II  $\lambda 4686$ , we also fit for the [ArIV] lines at 4711 and 4740 Å. The position of all lines is indicated by dotted vertical lines, with labels for their name. In this case, the ratio between the Gaussian model amplitude and the level of noise in the residuals, A/N, which relates to the detection level of the lines, is 2.7 for the He II  $\lambda 4686$ -line.

#### APPENDIX A: FITS FOR ALL SPECTRA

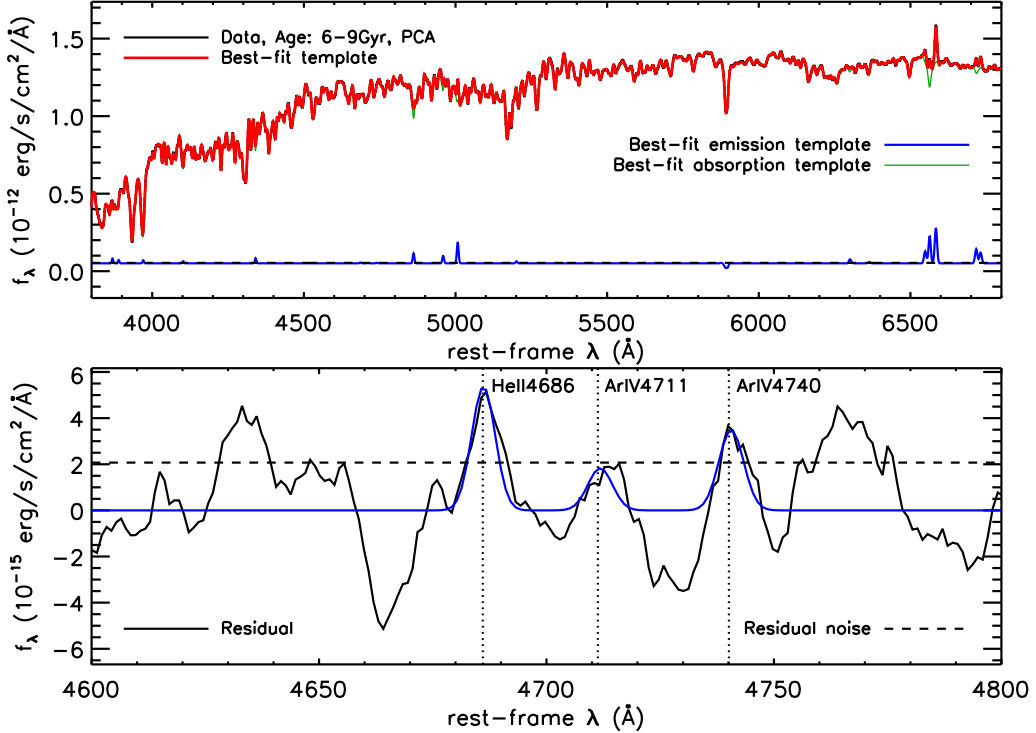
Figs. A1–A6 show the stacked spectra for our four age bins, together with their corresponding best-fitting stellar model. Overall, we obtain very satisfactory fits also for the stacked spectra of the subsamples. Furthermore, we nearly always find in the residuals between the data and the stellar model a clear Gaussian feature at the expected position of the He II  $\lambda 4686$  line, which can be well matched using the same best-fitting line profile as that of the strong [N II]  $\lambda\lambda 6548, 6584$  lines. Only for the stacked spectrum corresponding to our oldest age bins (Fig. A4 and A6), we find a less regular and somewhat broader positive feature in the residuals between the data and stellar model. Hence, the estimated He II  $\lambda 4686$  line flux of the oldest age bin should probably be regarded as an upper limit.

The values of the A/N ratio for the He II  $\lambda 4686$  lines always fall in the range between 2.6 and 3.0 (see Table 3). Given that there is less than 1% probability of measuring A/N values around 2.4 or above just by chance in the wavelength region around the He II  $\lambda 4686$  line (see Section 4.2), this line is robustly detected also in the stacked spectra for the groups of galaxies with different luminosity-weighted stellar ages.

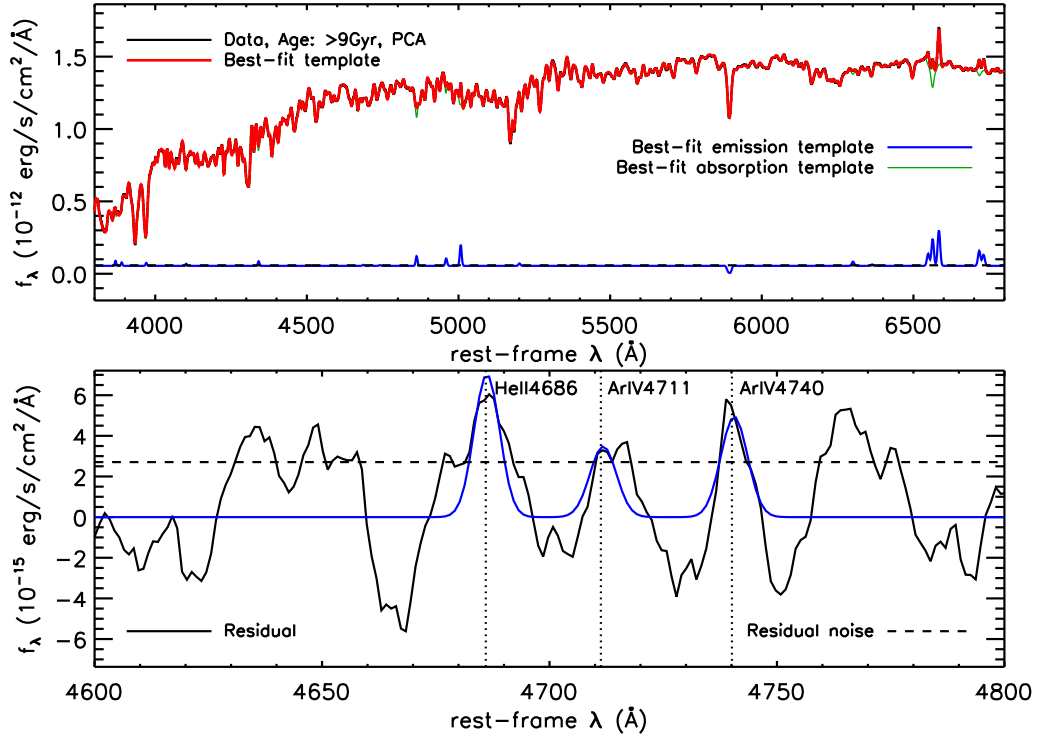
To evaluate the fits in more detail, Fig. A7 shows the fit around He II  $\lambda 4686$  (left hand side of each panel) and H $\beta$  and [O III] (right hand side of each panel) for each stacked spectrum, including best-fit overall template (red spectra), best-fit emission template (blue spectra) and best-fit stellar template (green spectra). We conclude that the quality of the fit is very high in these wavelength regimes. Moreover, to evaluate the effect of the polynomial correction (see Section 3.2), the top panel of Fig. A8 shows the best-fit template with (red spectrum) and without (black spectrum) polynomial correction, for the choice of stacking all individual spectra using the PCA criterion (see Section 2). The lower panel of Fig. A8 instead shows the polynomial correction as a function of wavelength, which shows a behavior close to being linear over the fitted wavelength range. Weak corrections on smaller scales are present, possibly due to flux calibration issues and template mismatch, but the polynomial correction is clearly dominated by the effects of reddening due to dust. Very similar results are found for all stacked spectra.



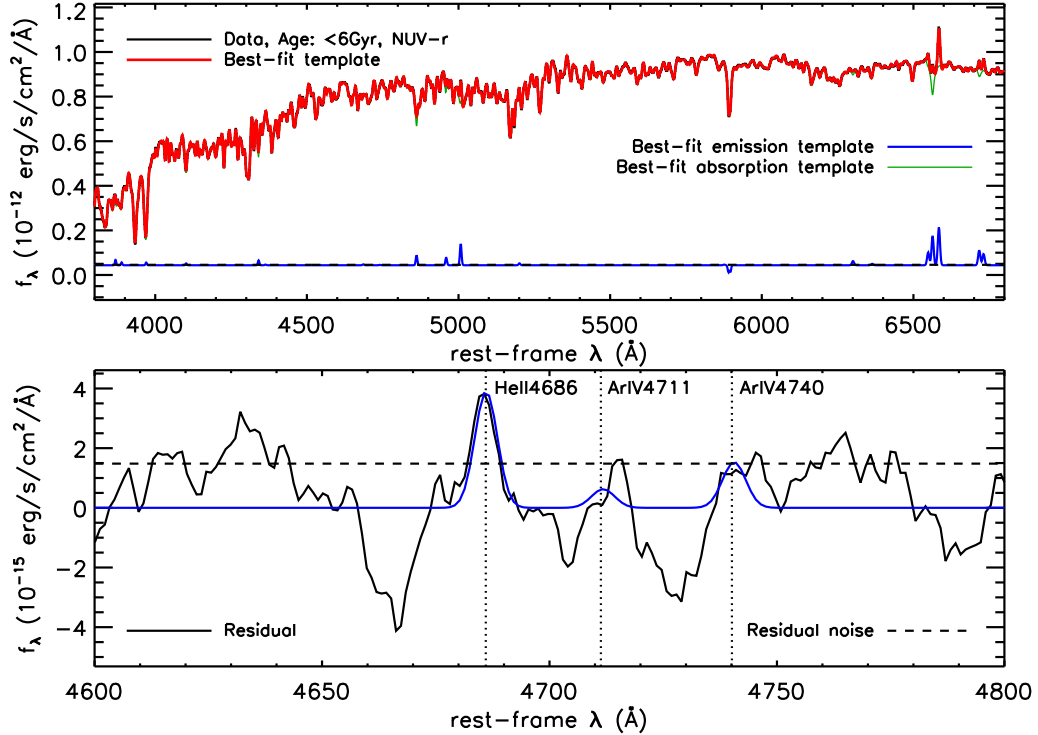
**Figure A2.** Same as Fig. 5 in the main manuscript and Fig. A1, but for the spectrum obtained by co-adding the spectra of all galaxies in our sample with luminosity-weighted mean stellar ages between 4 and 6 Gyr (3380 objects) and selected using the PCA criterion (see Section 2). The fit to the He II  $\lambda 4686$  line has an  $A/N=3.0$ .



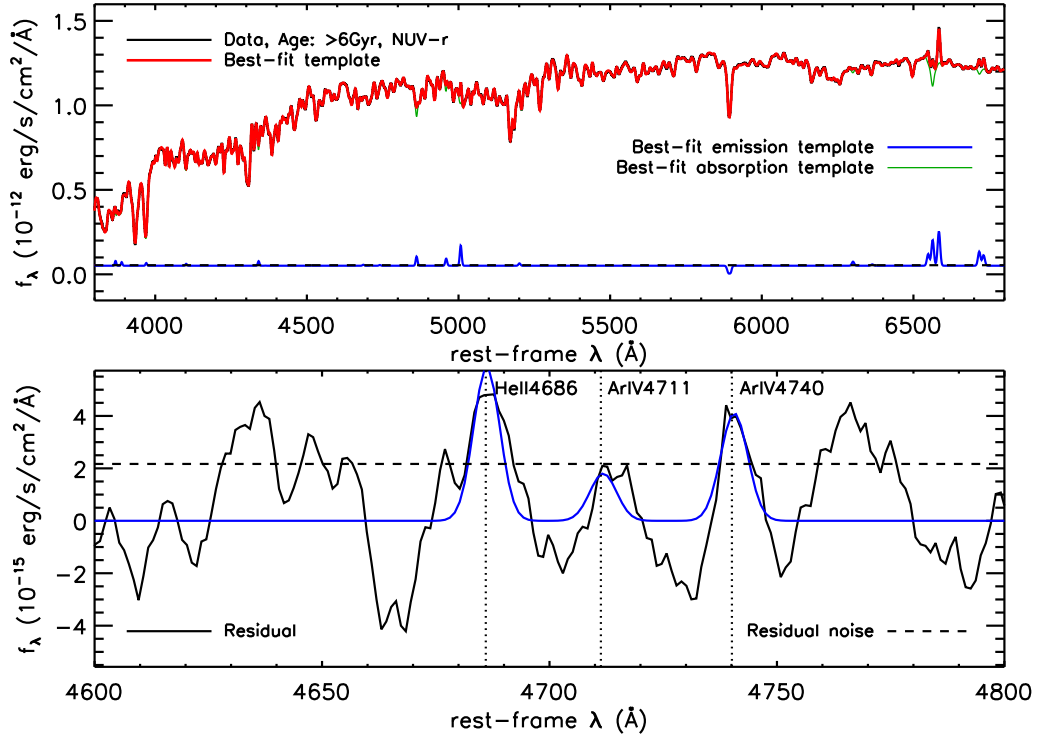
**Figure A3.** Same as Fig. 5 in the main manuscript and Figs. A1-A2, but for the spectrum obtained by co-adding the spectra of all galaxies in our sample with luminosity-weighted mean stellar ages between 6 and 9 Gyr (2729 objects) and selected using the PCA criterion (see Section 2). The fit to the He II  $\lambda 4686$  line has an  $A/N=2.6$ .



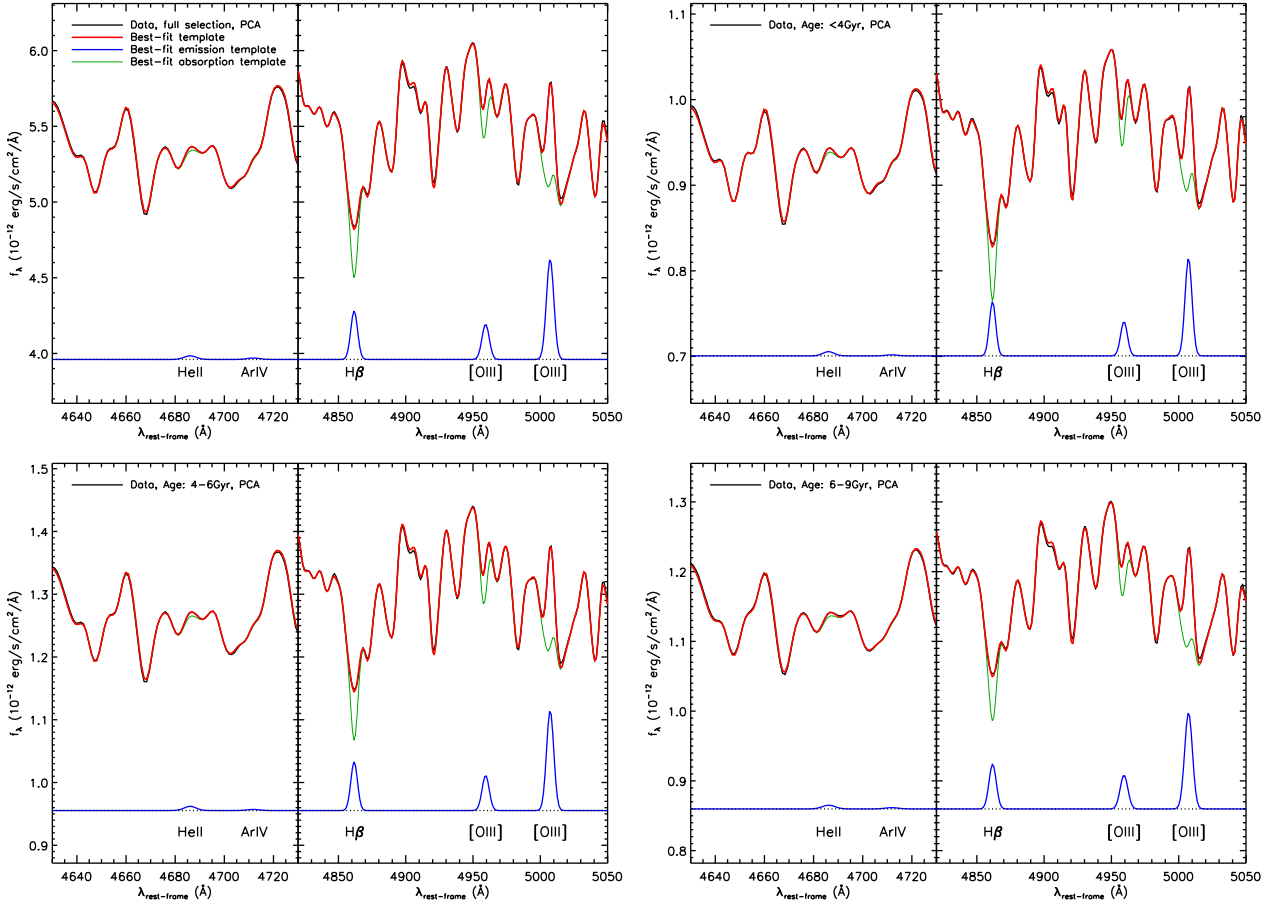
**Figure A4.** Same as Fig. 5 in the main manuscript and Figs. A1-A3, but for the spectrum obtained by co-adding the spectra of all galaxies in our sample with luminosity-weighted mean stellar ages  $>9$  Gyr (2744 objects) and selected using the PCA criterion (see Section 2). The fit to the He II  $\lambda 4686$  line has an  $A/N=2.6$ .



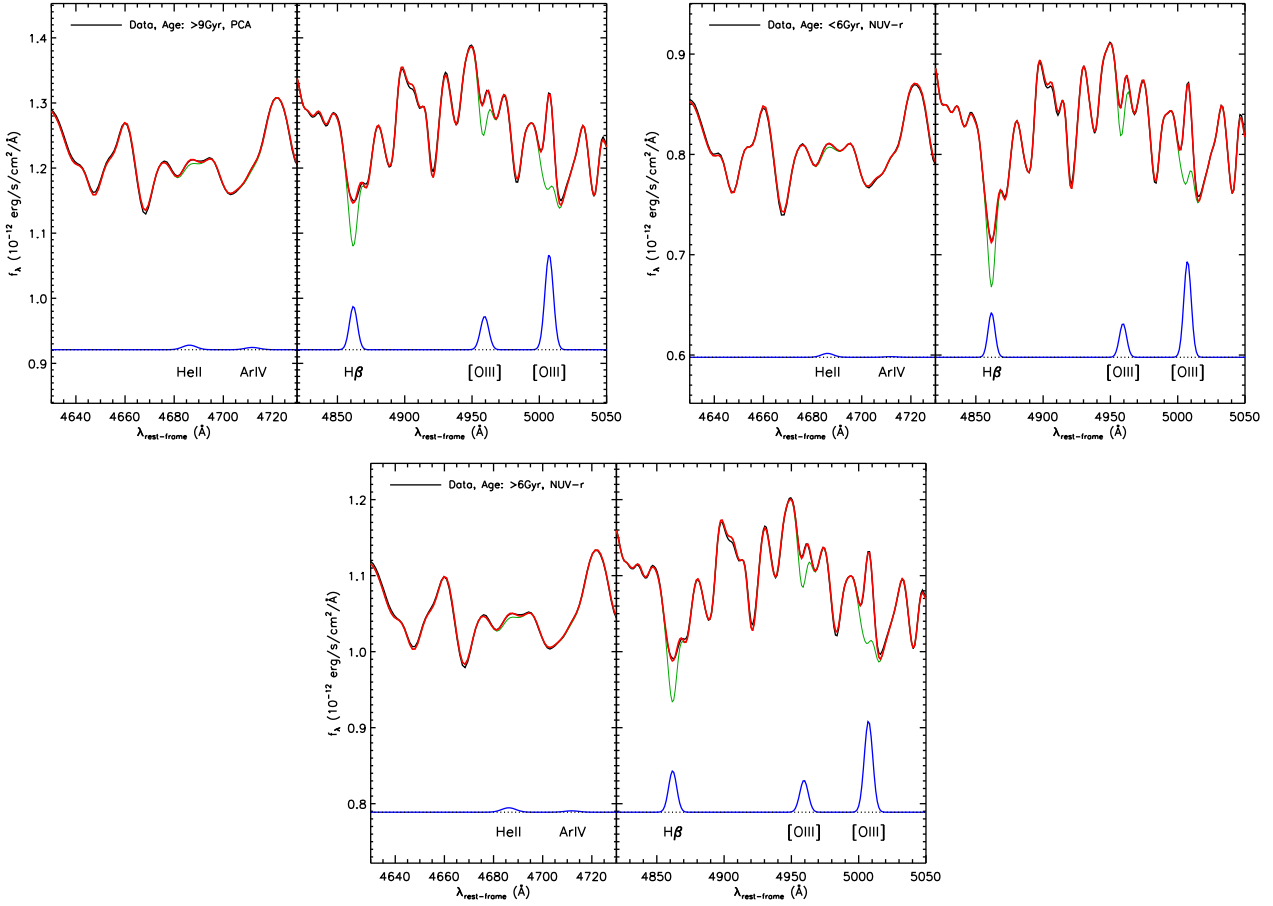
**Figure A5.** Same as Fig. 5 in the main manuscript and Figs. A1-A4, but for the spectrum obtained by co-adding the spectra of all galaxies in our sample with luminosity-weighted mean stellar ages  $<6$  Gyr (1953 objects) and selected using the NUV-r criterion (see Section 2). The fit to the He II  $\lambda 4686$  line has an  $A/N=2.7$ .



**Figure A6.** Same as Fig. 5 in the main manuscript and Figs. A1-A5, but for the spectrum obtained by co-adding the spectra of all galaxies in our sample with luminosity-weighted mean stellar ages  $>6$  Gyr (2108 objects) and selected using the NUV-r criterion (see Section 5). The fit to the He II  $\lambda 4686$  line has an  $A/N=2.6$ .



**Figure A7.** Zoom-in on the fit around He II  $\lambda 4686$  (left hand side of each panel) and H $\beta$  and [O III] (right hand side of each panel) for each of the stacked spectra (see label in the upper left corner of each panel).

**Figure A7 – continued**

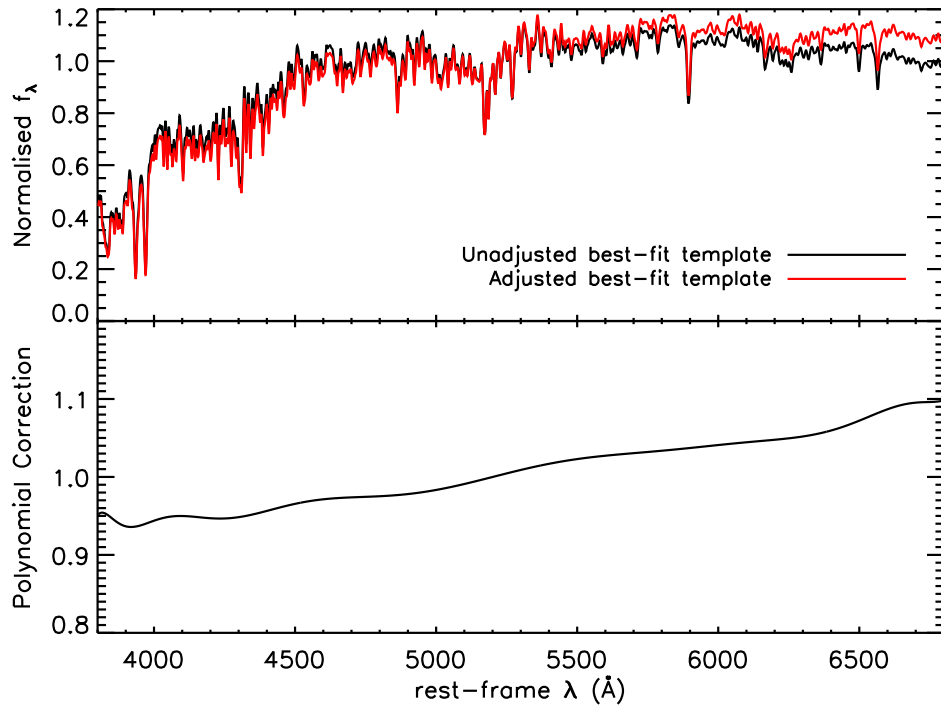


**Figure A8.** Top panel: Best-fit template with (red spectrum) and without (black spectrum) polynomial correction (see Section 3.2), for the choice of stacking all individual spectra using the PCA criterion (see Section 2). Lower panel: Polynomial correction as a function of wavelength.